Atmos. Chem. Phys. Discuss., 7, 13151–13173, 2007
www.atmos-chem-phys-discuss.net/7/13151/2007/

Atmospheric Chemistry and Physics Discussions

Cospectral analysis of high frequency signal loss in eddy covariance measurements

A. Wolf[1] **and E. A. Laca**[2]

[1]Carnegie Institution of Washington, Department of Global Ecology, Stanford CA, USA
[2]Department of Plant Sciences, U.C. Davis, Davis CA 95616, USA

Received: 30 July 2007 – Accepted: 31 August 2007 – Published: 7 September 2007

Correspondence to: A. Wolf (adamwolf@stanford.edu)

Abstract

The cospectra of momentum (M), sensible heat (H), latent heat (LE), and carbon dioxide (Fc) fluxes measured by eddy covariance (EC) over a shortgrass steppe are calculated for over 800 time intervals spanning a range of wind, surface heating, evaporative, and photosynthetic conditions. The power spectrum of the vertical wind clearly shows that the inertial subrange is not sufficiently captured. The cospectra of the different fluxes show that the lack of measurement resolution in the high frequency results in a loss of flux, especially as stability approaches neutral. A procedure is outlined to use statistics from the cospectrum to estimate the amount of high-frequency flux that remains unmeasured for each time interval. The greatest loss of flux was for H (14% on average for 0>z/L>0.001 where z/L is the dimensionless stability), consistent with other studies which indicate temperature fluctuations actively produce turbulence at high frequencies. LE and Fc showed less than half as much loss of flux as H. This differential loss of flux has direct implications for addressing energy balance closure in EC studies, as well as reconciling biases of fluxes measured by EC with the Modified Bowen Ratio technique. It is recommended that the cospectra of fluxes be examined while setting the height of instrumentation in order to insure that high frequency eddies are resolved.

1 Introduction

The eddy covariance (EC) technique has been an important development toward understanding plant growth and energy balance at the spatial scale of entire ecosystems and over a range of temporal scales (Baldocchi et al., 2001). In particular, EC emerged at a time when data on ecosystem-scale carbon balance was needed to constrain models of climate change (Goulden et al., 1996) and subsequent to the key development of a leaf model linking photosynthesis with transpiration and energy balance (Collatz et al., 1991). This combined model has been widely adopted in various forms into land

ACPD

7, 13151–13173, 2007

surface models (LSMs) used to provide surface boundary conditions to global carbon-climate models (GCMs) (e.g. Bonan and Levis, 2006; Dickinson et al., 2002; Sellers et al., 1996). Thus, the most widespread use of EC data is in calibrating LSMs against instantaneous hourly fluxes of CO_2, water, and heat, (hereafter collectively known as "fluxes") and integrated annual sums of water and carbon calculated from the processed EC data (Stockli and Vidale, 2005). The unbiasedness of the data collected using EC is then of paramount importance, because it serves as the foundation for a large number of research endeavors at plot, regional, and global scales.

The flux "data" made available by EC is in fact a highly processed statistic that has been manipulated in many ways using a host of theoretical considerations necessary to correct for different physical phenomena that can bias the calculated flux due to departures from several assumed conditions. One such assumption is that the measurements capture all scales of mixed-layer turbulence, but are not contaminated by mesoscale eddies or diurnal patterns, which introduce covariance between the wind and scalars that is independent of turbulence or local surface exchange. This requires measurements to be at a high enough frequency to capture fine-scale eddies, and extend long enough to capture low-frequency turbulent eddies out to some frequency where turbulent exchange is negligible. In practice, the high frequency limit is determined by the instrumental response time (<1 s), and the low frequency end of the observations is bounded by the averaging interval for which the flux is calculated (5–60 min). There is a well-founded theoretical (Lumley, 1964) and empirical (Kaimal et al., 1972; Vickers and Mahrt, 2003) justification for the existence of this frequency interval, judged on the basis of the spectral decomposition of the covariance of any scalar and the vertical wind. This quantity is known as the cospectrum (Wyngaard and Cote, 1972), and just as the product of a scalar and the vertical wind in the time domain equates to the flux of that scalar for that time interval, the cospectrum shows the scalar flux contained in eddies of that characteristic frequency interval.

Several aspects of the cospectrum deserve attention, because the cospectrum can be used as the basis to correct for undetected fluxes caused by limitation in the mea-

surements of vertical wind frequencies. The asymptotic behavior at the low frequency end is known as the "cospectral gap", and its shape can be affected by the length of time used to compute the fluxes and the choice of averaging technique used in Reynolds decomposition (Foken et al., 2006; Massman, 2000; Moore, 1986). The asymptotic behavior at the high frequency end is known as the "inertial subrange", where turbulent energy in large eddies is gradually dissipated into smaller eddies until the cospectrum reaches 0, i.e. the molecular diffusive limit. Many small-scale processes can affect the shape of the inertial subrange: signal asynchrony, instrument native frequency response, signal filtering, path-length averaging, sensor separation, and others. In addition to the shape of the cospectrum, the peak can vary under different conditions. In particular, the peak of the cospectrum is linked to the height at which the flux measurements are taken. Because the ground imposes a limit to the size of the eddies measured by the sensor, measurements closer to the surface tend to have cospectra that are shifted more toward the high frequency than measurements from taller towers (Rissmann and Tetzlaff, 1994).

Theoretical treatments conclude the slope of the cospectrum in the inertial subrange in log-log space is −7/3, and when each bin of the cospectrum is weighted by its frequency f, the slope becomes −4/3 (Wyngaard and Cote, 1972). The integral of the cospectrum is equal to the covariance, so cospectra are commonly normalized by their corresponding covariances, such that the area under the f-weighted cospectrum in semilog space is 1. For the remainder of this paper, all cospectra presented will be f-weighted and normalized by their covariance, so that cospectral area directly corresponds to proportion of flux carried by eddies of given frequency. Theory suggests that all scalars should be similar in their cospectral behavior, so that the normalized cospectra of momentum (M), heat (H), latent heat (LE), and CO_2 fluxes (Fc) should all take on the same peak and asymptotic shape for the same measurement conditions (Anderson and Verma, 1985; Kaimal et al., 1972; Wyngaard and Cote, 1972).

Kaimal et al. (1972) showed that the shape and position of power spectra and cospectra is closely dependent on the stability of the mixed layer, expressed as the

dimensionless stability parameter z/L, where L is the variable Obukhov length, and z is the fixed observation height (Kaimal and Finnigan, 1994). The stability parameter z/L characterizes the relative importance of buoyancy and shear in producing turbulence, where buoyancy causes z/L to become negative, stability causes z/L to become positive, and shear causes the z/L to become small. In general, stable conditions ($z/L>0$) prevail at night, when there may be large shear ($z/L\sim0$), or small shear ($z/L\gg0$) accompanying the negative heat flux. By contrast, the typically positive heat flux during the day leads to generally unstable conditions ($z/L<0$), although high shear will also drive z/L to near zero.

In this paper we examine the cospectra of M, H, LE, and Fc from a typical field experiment (Wolf et al., 2006) to determine whether the cospectra fulfill their expected properties, namely that they converge to zero at the cospectral gap, that they decay by −4/3 power to zero in the inertial subrange, and that all scalars are similar in their cospectral shape. We then examine the bias in the fluxes caused by flaws in the cospectra, identify measurement conditions that introduce bias, and present a procedure to correct measurements that are potentially biased.

2 Methods

2.1 Measurements

Measurements took place in five intervals of several days each from May to September 2001. The data represent a wide range of meteorological conditions during that period, including day, night, wet, dry, growing, and senescent periods. The study site was located in the shortgrass steppe region of Kazakhstan, 40 km north of the capital Astana, on the experimental station of the Baraev Kazakh Research Institute for Grain Crops Research. The field itself was a 200 ha pristine grass-forb steppe at 51.5758 N, 71.2681 E, 428 m above sea level. The fetch for upwind directions were 250 m from the north, 610 m from the east, 2250 m from south, and 360 m from the west, beyond

which were fallow wheat fields. The site is extraordinarily flat, with no slopes exceeding 0.5° for 20 km in any direction, and only isolated trees, with none nearer than 5 km. The canopy height was approximately 0.3 m. A description of the ecology and meteorology of the site is available in Wolf et al. (2006).

Fluxes of CO_2, water, heat, and momentum were measured using an eddy covariance system based on a fast-response open-path infrared gas analyzer (IRGA; model LI-7500, Licor, Inc. Lincoln, NE) coupled with a 3-dimensional sonic anemometer (model CSAT-3, Campbell Scientific, Logan, UT), both installed at 1.3 m above ground level. Digital signals from these instruments were recorded at 10 Hz using a Campbell Scientific CS5000 datalogger. All raw data were archived for later post-processing.

2.2 Data processing

Data were processed in several steps to compute either fluxes or cospectra. The steps in flux processing were (1) parsing data into 20 min intervals; (2) recursively removing spikes greater than 6 σ beyond a quadratic fit to the 10 Hz data; (3) dealiasing with a 1st order Butterworth filter with a cutoff frequency at 4.8 Hz, which had the recurrence relation:

$$y_t = 0.94165478x_t + 0.94165478x_{t-1} - 0.8833089876y_{t-1} \quad (1)$$

(Fisher, N. D.) where x is the original scalar time series and y is the filtered time series; (4) rotation to a natural coordinate system (Lee et al., 2004); (5) removing signal asynchrony by maximizing the covariance between each scalar and the vertical wind (e.g. Eugster et al., 1997); (6) calculating scalar fluxes using the mean and covariance of each scalar with the vertical wind; (7) making frequency domain corrections to the fluxes for path-length averaging using the filter coefficients summarized in Massman (2000); and (8) adjusting fluxes for air density artifacts (Webb et al., 1980).

Calculation of power spectra and cospectra was identical for steps 1–5, after which (6b) power spectra and cospectra were calculated and aggregated into 23 frequency bins; and (7b) cospectra for each scalar (denoted generically x below) were divided by

ACPD
7, 13151–13173, 2007

the transfer function H_x for each frequency bin (f), using filter coefficients (τ) for each instrument's sensor separation distance:

$$\tau_{wC,wQ} = \sqrt{\tau_{\mathrm{IRGA}} + \tau_{\mathrm{CSAT_Z}}} \tag{2}$$

$$\tau_{wU} = \sqrt{\tau_{\mathrm{CSAT_Z}} + \tau_{\mathrm{CSAT_{XY}}}} \tag{3}$$

$$\tau_{wT} = \sqrt{\tau_{\mathrm{CSAT_Z}}} \tag{4}$$

$$H_x(f) = (1 + 2\pi f \tau_{wx})^{-1} \tag{5}$$

$$Co(wx)' = Co(wx)/H_x \tag{6}$$

where $Co(wX)$ refers to the cospectrum of wX, where w is the vertical wind and X is a generic scalar (e.g. U for streamwise horizontal wind, T for temperature, Q for H_2O, and C for CO_2). The subscripts to τ refer to the instruments used to measure the scalars, including an infrared gas analyzer (IRGA) for CO_2 and H_2O, and a sonic anemometer (CSAT) for horizontal (x) and vertical (z) components of the wind. The transfer functions increase the high frequency part of the cospectrum (Fig. 1). Finally, the frequencies were transformed into the dimensionless frequency $\eta = fz/U$, and each cospectrum divided by its corresponding flux.

2.3 Analyses of cospectra

Once normalized cospectra were obtained, several quantities were subsequently calculated (Fig. 2), presented below using MATLAB syntax (MathWorks, 2005). The slope of the final four bins of cospectra was calculated using least squares in log-log units (where all logs use base 10):

$$[\mathrm{slope}, \mathrm{intercept}] = \mathrm{polyfit}(\log 10(f), \log 10(CoWX), 1); \tag{7}$$

ACPD
7, 13151–13173, 2007

Subsequently, two points were calculated: the point (xN, yN) at which the regression from the observed cospectrum reached the Nyquist frequency fN:

$$yN = 10.\hat{}(\log(fN). \times \text{slope} + \text{intercept}); \quad (8)$$

$$xN = fN; \quad (9)$$

and the point (xT, yT), where a −4/3 slope (in log-log units) extending from (xN, yN) would reach a negligible value, nominally 10^{-3}:

$$yT = 10.\hat{} - 3; \quad (10)$$

$$d\text{Log}Y = \log(yT) - \log(yN); \quad (11)$$

$$xT = fN \times 10\hat{}(d\text{Log}Y/(-4/3)) \quad (12)$$

The area under the curve defined by these two points was called the "lost flux" and calculated as:

$$k = \log 10(yN \times xN\hat{}(4/3)); \quad (13)$$

$$a = 0.0380965430607922; \quad (14)$$

$$b = 0.325720861427438; \quad (15)$$

$$\text{LostFlux} = 10\hat{}k \times (a - b/10\hat{}((4 \times \log 10(xT))/3)); \quad (16)$$

3 Results

The distribution of stability parameter z/L over the day is presented in Fig. 3. Although there are never unstable periods of night, there are occasionally stable periods during the day, typically accompanying precipitation events. The magnitude of z/L is greater

ACPD
7, 13151–13173, 2007

during stable periods than unstable periods, indicating a generally low surface heat flux during the day, but strong nocturnal inversions, and generally high shear at the site.

The power spectra for the vertical wind (w) are sorted from left to right in the low frequency range from unstable to stable (Fig. 4), similar to the classic results of Kaimal et al. (1972). However, nearly all of the data lie in the range $-0.1<z/L<0.1$, and when this range is subdivided into finer bins than in Kaimal et al. (1972), we see an additional source of variability among the power spectra. As the stability approaches zero, the peak shifts to higher frequencies, with the consequence that less and less of the inertial subrange of the turbulence is observed.

Exploring this phenomenon further, the height of the final bin of the power spectrum can be taken as a metric of how much of the inertial subrange of turbulence has been resolved by the measurements. As the stability approaches zero from either direction, the peak of the power spectrum $S(w)$ is shifted toward fN, and the value of $S(w)$ at fN increases toward the peak value. By this metric, the most neutral observation periods clearly resolve the least high frequency turbulence (Fig. 5).

The cospectra for M, H, LE, and Fc show several clear dependencies with stability (Fig. 6). As z/L moves from very unstable to very stable, the cospectra become more peaked, and shift to higher frequencies. This indicates that in very stable air the turbulent eddies are smaller in general and more constrained in their size distribution. The different scalars appear subtly different from one another, most particularly in the descent toward the inertial subrange. M and H do not descend as far to zero as LE and Fc by the time the cospectra reach the Nyquist frequency, apparently a consequence of a slight shift in the M and H cospectra toward the right relative to LE and Fc. This increase in power at high frequencies for H has been attributed by others to temperature fluctuations leading to buoyant production of turbulence (Katul et al., 2001). The difference in the cospectrum of turbulent exchange of the different scalars indicates that the temperature fluctuations likely originate in different locales in the canopy from water vapor and CO_2 fluctuations.

As a consequence of cospectral peak shifting under different stability regimes, the

high frequency termini of the cospectra vary with respect to their final height and frequency. The most neutral spectra are relatively low frequency, and also furthest from zero power, with the consequence that the unresolved region of the inertial subrange is largest in these most neutral conditions. These characteristics of the high frequency termini of the cospectra are presented for the heat flux in Fig. 7.

The lost flux region clearly peaks as z/L approaches neutral from either direction (Fig. 7c), as a consequence of the peak shifting closer to the Nyquist frequency of the measurements (Fig. 7b). While the majority of observation periods have losses below 5%, a substantial number have 10% or greater losses. The slope of the final bins of the cospectrum approaches zero as the stability approaches zero (Fig. 7d), indicating that these comprise the crest of the cospectral peak at neutrality. Interestingly, few of the heat flux cospectra appear to conform to the expected −4/3 slope, and tend toward a −2/3 slope.

Cospectra for all the fluxes were similarly analyzed for the dependence of the lost flux on stability, and the same general pattern holds, in which the most neutral measurements have the greatest losses (Fig. 8). However, there are clear differences in the amount of high frequency flux loss between the different scalars. For conditions where $0<z/L<0.001$, H suffers the most flux loss (5–14%) in the region $-0.1<z/L<0.1$, followed by M, but LE and Fc never lose more than a few percent (2–5%).

It has been suggested that if the instruments are not filtered between the signal measurement and subsequent logging, then the high frequency noise will be aliased back into the signal. This appear to be the case, as the power spectra of the unfiltered data show a slight increase in power at the highest frequencies (data not shown). Nonetheless, this does not mean that the aliased fluctuations contained in two signals should co vary. In other words, if any of the turbulent flux is contained in eddies that co vary at frequencies beyond the measurement frequency, they are lost. To demonstrate that changing the sampling frequency decreases the total turbulent flux that is measured, I degraded the signal by sampling the real signals at 1/2, 1/3, ... 1/10 the true sampling frequency, and calculated the fluxes using the procedure above to determine the loss

ACPD
7, 13151–13173, 2007

of signal. Because the signals are not averaged in this process, they should contain some of the high frequency variations of the native resolution. The drop from 10 Hz to 5 Hz to 3.3 Hz show a strong loss of signal, up to a loss of ~10% of the flux from H, LE and Fc (Fig. 9). The M flux was not very affected by degrading the signal. This reconfirms that the combination of the measurement height, the surface roughness, the wind speed, and the measurement frequency are characterizing a region of turbulence that is very sensitive to changes in the measurement frequency.

4 Discussion

This research was begun as attempt to understand lack of energy balance in EC studies. Studies to date have preferred to assign the undermeasurement to the LE flux, because H_2O is measured by a separate instrument from T and w (Twine et al., 2000). This logic implies that the CO_2 flux is also undermeasured, because it too is measured separately from T and w. Another line of argument suggests that perhaps the Bowen ratio (H/LE) is accurately measured by the instrument, but that sum of H and LE is undermeasured (Twine et al., 2000). This argument would appear to be false, as side-by-side comparisons between EC and Modified Bowen Ratio techniques show clear differences in their Bowen ratios (Brotzge and Crawford, 2003). Still another consideration of energy balance non closure (Foken et al., 2006) attributes the error to losses in the low-frequency part of the turbulence spectrum. The study in this paper indicates that undermeasurement of the H flux may well be more at fault in energy balance closure, that the Bowen ratio may not be accurately measured by EC, and that the high frequency part of the spectrum may be at issue in some studies. The method shown for calculating the loss of the high frequency flux can be directly applied to any set of fluxes for which the raw high frequency data has been kept, and can directly address this loss of flux.

The more important lesson in this study is that flux towers need to be high enough above the canopy to be able to resolve all of the turbulence. Although the tower was

over 5 times the height of the canopy, the failure of the instrument setup to capture all the relevant scales of turbulence is a major compromise to the goal of accurately measuring the intended fluxes. This failure could be avoided by checking cospectra under high shear conditions and confirming that they do indeed taper off to near zero at the Nyquist frequency.

Acknowledgements. We gratefully acknowledge R. Street, and D. Leschow and especially I. Faloona for discussions that greatly enhanced this work. This publication was made possible through support provided by U.S. universities, host country institutions and the Office of Agriculture and Food Security, Global Bureau, U.S. Agency for International Development, under grant PCE-G-98-00036-00. The opinions expressed herein are those of the author(s) and do not necessarily reflect the views of USAID.

References

Anderson, D. E. and Verma, S. B.: Turbulence Spectra of CO2, Water-Vapor, Temperature and Wind Velocity Fluctuations over a Crop Surface, Bound.-Lay. Meteorol., 33(1), 1–14, 1985.

Baldocchi, D., Falge, E., Gu, L. H., et al.: FLUXNET: A new tool to study the temporal and spatial variability of ecosystem-scale carbon dioxide, water vapor, and energy flux densities, Bull. Am. Meteor. Soc., 82(11), 2415–2434, 2001.

Bonan, G. B. and Levis, S.: Evaluating aspects of the community land and atmosphere models (CLM3 and CAM3) using a Dynamic Global Vegetation Model, J. Climate, 19(11), 2290–2301, 2006.

Brotzge, J. A. and Crawford, K. C.: Examination of the surface energy budget: A comparison of eddy correlation and Bowen ratio measurement systems, J. Hydrometeorol., 4(2), 160–178, 2003.

Collatz, G. J., Ball, J. T., Grivet, C., and Berry, J. A.: Physiological and Environmental-Regulation of Stomatal Conductance, Photosynthesis and Transpiration – a Model That Includes a Laminar Boundary-Layer, Agr. Forest Meteorol., 54(2–4), 107–136, 1991.

Dickinson, R. E., Berry, J. A., Bonan, G. B., et al.: Nitrogen controls on climate model evapotranspiration, J. Climate, 15(3), 278–295, 2002.

Eugster, W., Mcfadden, J. P., and Chapin, E. S.: A comparative approach to regional variation in

surface fluxes using mobile eddy correlation towers, Bound.-Lay. Meteorol., 85(2), 293–307, 1997.
Fisher, A. J. N. D.: Interactive Digital Filter Design, York, UK, University of York, Dept. of Computer Science, http://www-users.cs.york.ac.uk/~fisher/mkfilter, accessed March 2007.
Foken, T., Wimmer, F., Mauder, M., Thomas, C., and Liebethal, C.: Some aspects of the energy balance closure problem, Atmos. Chem. Phys., 6, 4395–4402, 2006, http://www.atmos-chem-phys.net/6/4395/2006/.
Goulden, M. L., Munger, J. W., Fan, S. M., Daube, B. C., and Wofsy, S. C.: Measurements of carbon sequestration by long-term eddy covariance: Methods and a critical evaluation of accuracy, Global Change Biol., 2(3), 169–182, 1996.
Kaimal, J. C. and Finnigan, J.: Atmospheric boundary layer flows: their structure and measurement, Oxford, New York, 289 pp, 1994.
Kaimal, J. C., Izumi, Y., Wyngaard, J. C., and Cote, R.: Spectral Characteristics of Surface-Layer Turbulence, Q. J. Roy. Meteor. Soc., 98(417), 563–589, 1972.
Katul, G., Lai., C.-T., Shafer, K., et al.: Multiscale analysis of vegetation surface fluxes: from seconds to years, Adv. Water Resour., 24(9–10), 1119–1132, 2001.
Lee, X. H., Finnigan, J., and U, K. T. P.: Coordinate systems and flux bias error, in: Handbook of Micrometeorology, edited by: Lee, X. H., Massman, W. J., and Law, B., Kluwer, Dordrech, 2004.
Lumley, J. L.: The Spectrum of Nearly Inertial Turbulence in a Stably Stratified Fluid, J. Atmos. Sci., 21(1), 99–102, 1964.
Massman, W. J.: A simple method for estimating frequency response corrections for eddy covariance systems, Agr. Forest Meteorol., 104(3), 185–198, 2000.
MathWorks, I.: MATLAB: the language of technical computing. Getting started with MATLAB, version 7. MarthWorks, Inc., Natick, MA, 2005.
Moore, C. J.: Frequency-Response Corrections for Eddy-Correlation Systems, Bound.-Lay. Meteorol., 37(1–2), 17–35, 1986.
Rissmann, J. and Tetzlaff, G.: Application of a Spectral Correction Method for Measurements of Covariances with Fast-Response Sensors in the Atmospheric Boundary-Layer up to a Height of 130 M and Testing of the Corrections, Bound.-Lay. Meteorol., 70(3), 293–305, 1994.
Sellers, P. J., Bounoua, L., Collatz, G. J., et al.: Comparison of radiative and physiological effects of doubled atmospheric CO2 on climate, Science, 271(5254), 1402–1406, 1996.
Stockli, R. and Vidale, P. L.: Modeling diurnal to seasonal water and heat exchanges at Euro-

pean Fluxnet sites, Theor. Appl. Climatol., 80(2–4), 229–243, 2005.
Twine, T. E., Kustas, W. P., Norman, J. M., et al.: Correcting eddy-covariance flux underestimates over a grassland, Agr. Forest Meteorol., 103(3), 279–300, 2000.
Vickers, D. and Mahrt, L.: The cospectral gap and turbulent flux calculations, J. Atmos. Ocean. Tech., 20(5), 660–672, 2003.
Webb, E. K., Pearman, G. I., and Leuning, R.: Correction of Flux Measurements for Density Effects Due to Heat and Water-Vapor Transfer, Q. J. Roy. Meteor. Soc., 106(447), 85–100, 1980.
Wolf, A., Akshalov, K., Saliendra, N., Johnson, D. A., and Laca, E. A.: Inverse estimation of Vc(max), leaf area index, and the Ball-Berry parameter from carbon and energy fluxes, J. Geophys. Res.-Atmos., 111(D8), S08, doi:10.1029/2005JD005927, 2006.
Wyngaard, J. C. and Cote, O. R.: Cospectral Similarity in Atmospheric Surface-Layer, Q. J. Roy. Meteor. Soc., 98(417), 590–603, 1972.

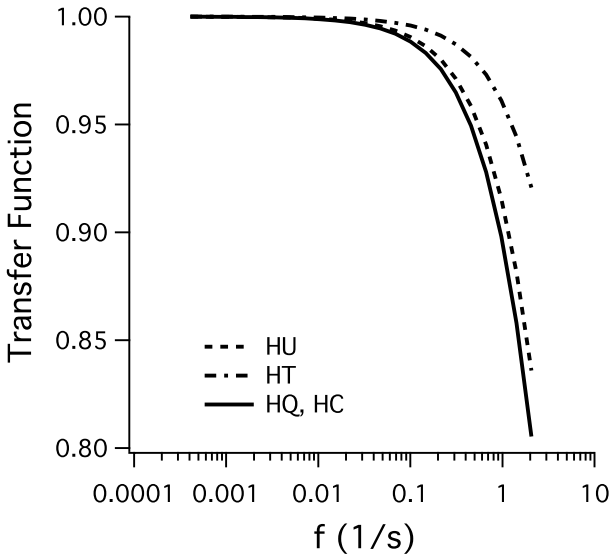

Fig. 1. Transfer function weights applied to cospectra to correct for path-length averaging of the measured scalars for a typical wind speed (2.9 m s^{-1}). The cospectral power at each frequency bin is divided by the corresponding Hx value to yield an estimate of the unfiltered cospectrum.

ACPD
7, 13151–13173, 2007

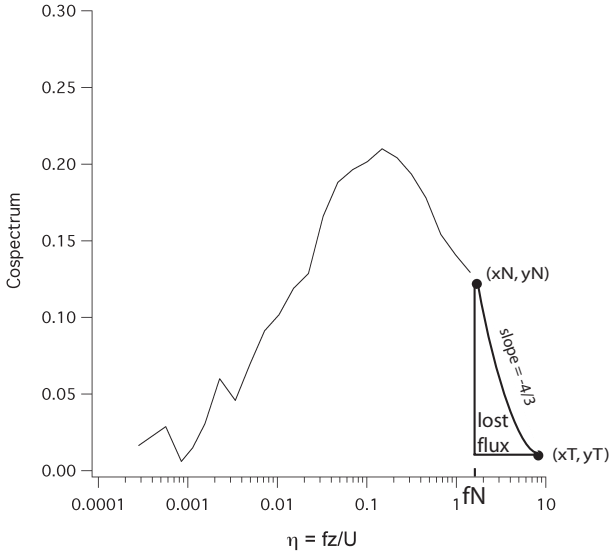

Fig. 2. Archetype of an observed cospectrum, showing the showing the terminal observed value of the cospectrum well above zero at the normalized Nyquist frequency (fN). Extending a line from this point to zero using a −4/3 slope shows an area of the flux in the inertial subrange that is unresolved by the measurement frequency, and is called here the "lost flux". That the plotted points of the cospectrum represent midpoints of bins in the observed cospectrum, so the terminal bin is bounded by fN on the high frequency end. Note that this graph is semilog, making the −4/3 slope non linear.

ACPD
7, 13151–13173, 2007

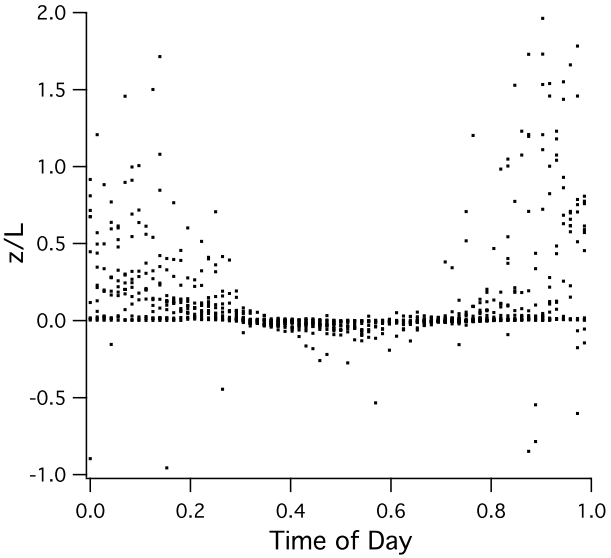

Fig. 3. Stability parameter z/L from the measurement periods used in the study. The time of day is shown as fraction of a day.

ACPD
7, 13151–13173, 2007

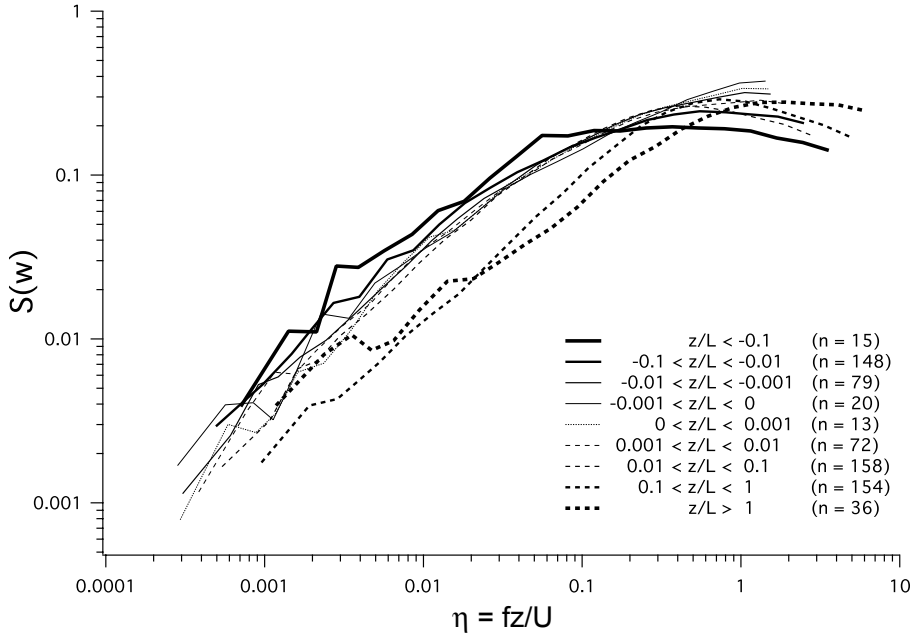

Fig. 4. The power spectrum of the vertical wind averaged within different stability regimes. Dashed lines are neutral to stable, and solid lines are neutral to unstable. Lines become thinner as they approach neutral. The number of observation periods represented by each stability bin are shown in parentheses.

ACPD
7, 13151–13173, 2007

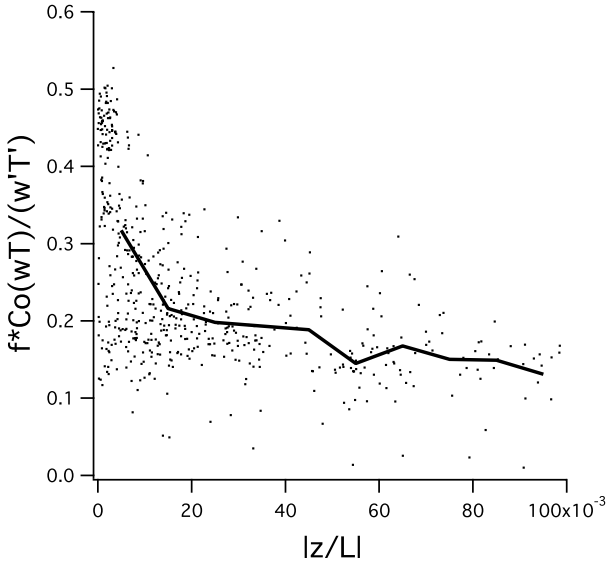

Fig. 5. The value of the power spectrum of w at the Nyquist frequency under different stability regimes. The diagram is symmetric, so z/L is expressed as an absolute value. The heavy line represents the average of 0.0001 increments of |z/L|.

ACPD
7, 13151–13173, 2007

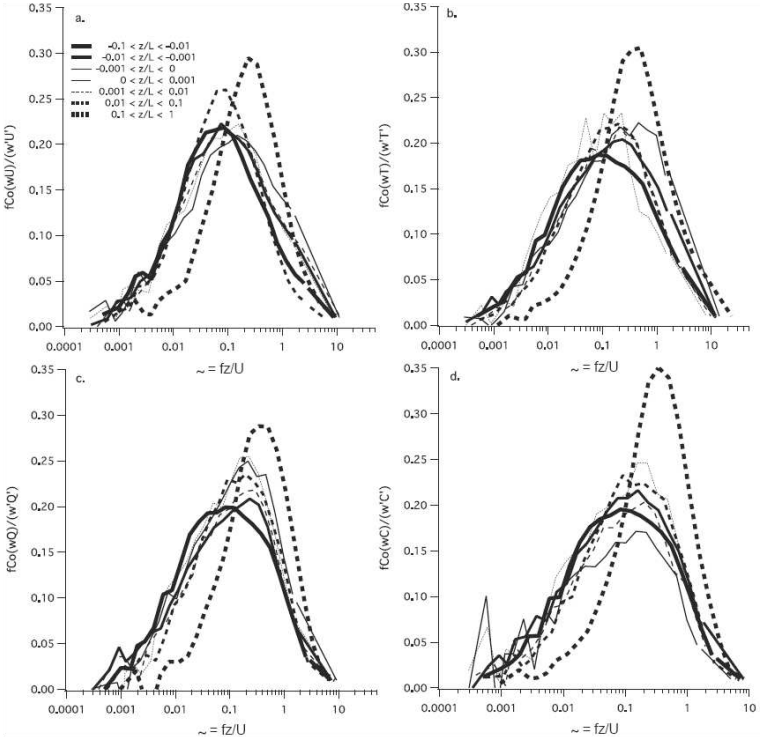

Fig. 6. The cospectrum of four vertical scalar fluxes: **(a)** momentum; **(b)** heat; **(c)** evaporation; **(d)** CO_2 exchange. Dashed lines are neutral to stable, and solid lines are neutral to unstable. Lines become thinner as they approach neutral. The number of observation periods represented by each stability bin are the same as in Fig. 3. The lines extending to the right from each cospectrum are estimates of the lost flux.

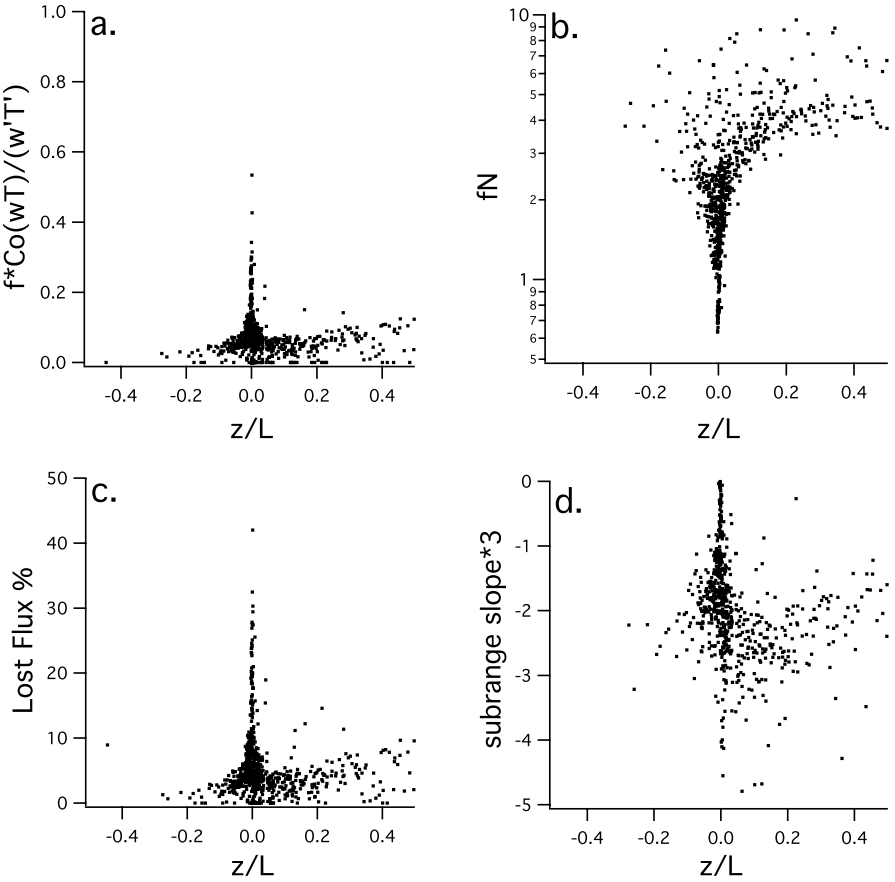

Fig. 7. Characteristics of the high frequency terminus of the observed cospectra of $w'T'$ under different stability regimes. **(a)** The final cospectral power (abscissa); **(b)** The normalized Nyquist frequency; **(c)** The lost flux calculated from the cospectrum, calculated by extending the final point on the cospectrum to zero using −4/3 slope; **(d)** The observed slope of the last four bins of the cospectrum, expressed in thirds.

ACPD
7, 13151–13173, 2007

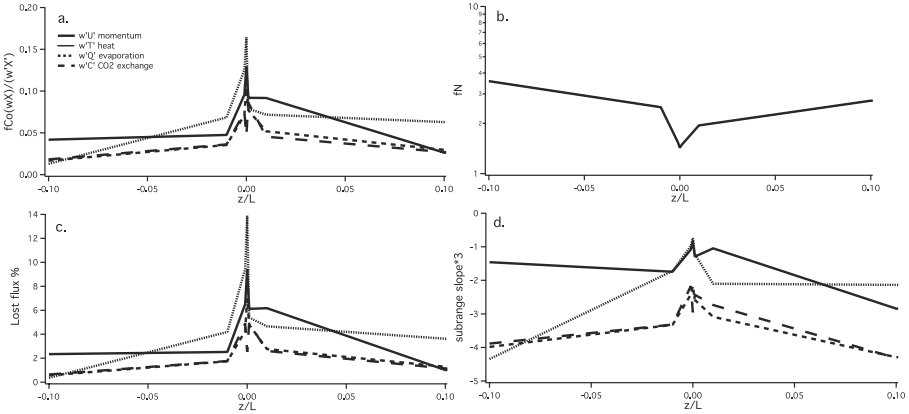

Fig. 8. Characteristics of cospectra of vertical fluxes of scalars under different stability regimes. **(a)** The value of the cospectrum at fN; **(b)** the normalized Nyquist frequency; **(c)** the lost flux; **(d)** the slope of the final four bins of the cospectra. The bins of z/L are the same as in Fig. 5, but plotted as the upper value of each bin (i.e. $-0.001>z/L>0$ is plotted at 0).

ACPD
7, 13151–13173, 2007

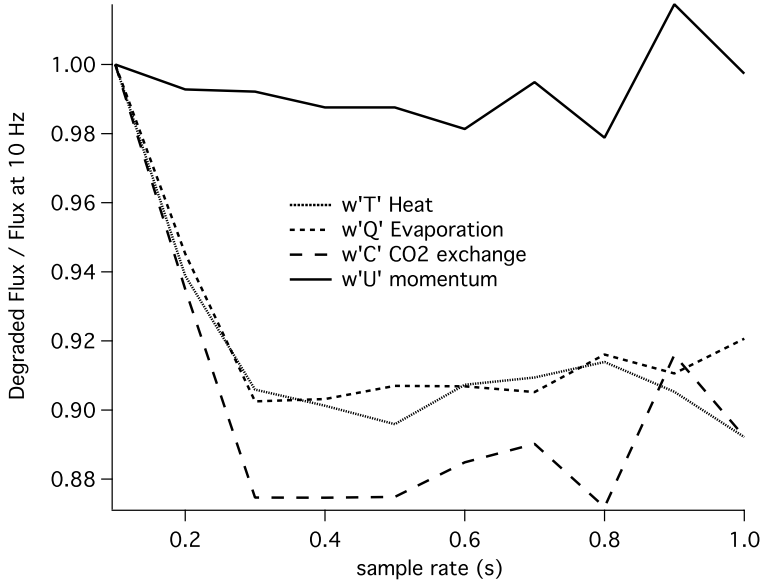

Fig. 9. Scalar fluxes calculated with reduced sampling rates, at 1/2, 1/3, ... 1/10 the native 10 Hz sampling rate, shown as a proportion of the flux at the native resolution.

ACPD
7, 13151–13173, 2007